Progress In Electromagnetics Research C, Vol. 89, 233–241, 2019

Compact Microstrip Diplexer Based on Dual Closed Loop Stepped Impedance Resonator

Salif N. Dembele[1, *], Jingfu Bao[1], Ting Zhang[1], and Denis Bukuru[2]

Abstract—A compact microstrip diplexer based on dual closed loop stepped impedance resonator (DCLSIR) is proposed. The proposed microstrip diplexer is composed of the combination of two DCLSIR bandpass filters (BPFs), which are designed for X-band application. For the demonstration, a dual-channel diplexer has been designed and fabricated using microstrip and printed circuit board (PCB) technologies, respectively. The fabricated diplexer, operating at 8.3/10 GHz for X-band application, has compact size (15.17 mm × 2.69 mm). The measured results are in good agreement with the full-wave simulation results. Good isolation between two channels is achieved.

1. INTRODUCTION

Diplexers are one of the most important components in microwave circuits for channel separation in modern wireless, mobile, satellite communications, and radar systems. They are usually designed using two or multiple BPFs to separate each frequency passband. To be suitable for application in the above-mentioned communications and systems, diplexers with high performance, compact size, light weight, low cost, and easy integration with other front-end circuitries simultaneously are highly demanded. Therefore, various techniques have been extensively studied to design diplexers. In [1], ridge waveguide has been used for diplexer applications. However, such waveguide design is challenging to be integrated directly within a planar system. The most common methods to form a planar diplexer are based on designing two BPFs separately with different frequencies, then using T-junction [2, 3], Y-junction [4, 5], common resonator [6, 7], and matching circuit [8, 9] to combine these two BPFs to form the final diplexer circuit. However, most of these diplexers are not small enough to be used.

The most technique used to compact the microstrip diplexer is to select proper resonators to reduce the circuit size since resonators are basic components of a filter. Thus, tri-mode stub-loaded resonator [10] and slotline stepped impedance resonator [11] have been used in diplexer configuration. Microstrip diplexers using TM_{010} circular cavity [12], folded open-loop ring resonators [13], stepped impedance resonators [14], and ring resonator [15] have also been designed to reduce the circuit area of the diplexer, but the aforementioned diplexers still have the disadvantage of large circuit area. Based on matching circuit approach [8, 9], microstrip diplexers have also been designed and reported for reducing the circuit area of the diplexer; however, the occupied area of the matching circuit limits efforts of the reduction of circuit area. Moreover, some microstrip diplexer configurations exhibit disadvantages such as harmonics near or inside the two passbands which will degrade performance of the diplexer [3, 16]. Therefore, the design of microstrip diplexers with compact size is still a great challenge.

In this paper, a compact microstrip diplexer based on dual closed loop stepped impedance resonator operating at X-band frequencies is proposed. Compact size and good isolation between the two passbands are achieved. The measured results are in good agreement with the simulated ones.

Received 6 November 2018, Accepted 22 December 2018, Scheduled 7 January 2019

* Corresponding author: Salif N. Dembele (salifnabounadembele@yahoo.fr).

[1] School of Electronic Science and Engineering, University of Electronic Science and Technology of China, Chengdu 611731, China.

[2] Department of Applied Science, Ecole Normale Superieure, Bujumbura 6983, Burundi.

2. DESIGN OF THE PROPOSED COMPACT MICROSTRIP DIPLEXER

2.1. Resonator Analysis for Diplexer

Figure 1(a) depicts the resonator of the proposed diplexer, which is formed by two closed-loop SIRs. P-P′ indicates the symmetry line of the resonator. Based on its symmetry, even-odd-mode technique can be applied to analyze the characteristics of the resonator. Under odd-mode excitation, the symmetric line P-P′ can be modeled as a perfect electric wall. The odd-mode equivalent transmission line model is indicated in Fig. 1(b). Under even-mode excitation, the symmetric line P-P′ behaves as a perfect magnetic wall. The even-mode equivalent transmission-line model is shown in Fig. 1(c). The odd-mode resonant frequency f_{od} and even-mode resonant frequency f_{ev} are functions of parameters of the resonator, which can be expressed as:

$$f_{od} = \frac{c}{L_{od}\sqrt{\varepsilon_{eff}}}, \tag{1}$$

$$f_{ev} = \frac{c}{L_{ev}\sqrt{\varepsilon_{eff}}}, \tag{2}$$

where

$$L_{od} = (L_1)/4 + (L_2 + L_3)/2, \tag{3}$$

$$L_{ev} = (L_1)/2 + (L_2 + L_3), \tag{4}$$

c is the light speed in free-space, and ε_{eff} is the effective dielectric constant of the substrate.

Subsequently, only the odd-mode has been considered to analyze the equivalent transmission line model of the proposed resonator. As shown in Fig. 1, Z_1, Z_2, and Z_3 indicate characteristic impedances of the transmission line of electrical lengths θ_1, θ_2, and θ_3, respectively. The impedance ratio is defined as:

$$R_z = \frac{Z_1}{Z_2} = \frac{Z_3}{Z_2}, \tag{5}$$

and the odd-mod input impedance is expressed as [1, 7]:

$$Z_{od} = Z_1 \frac{Z_{loop} + jZ_1 \tan\left(\frac{\theta_1}{4}\right)}{Z_1 + jZ_{loop} \tan\left(\frac{\theta_1}{4}\right)}, \tag{6}$$

where

$$Z_{loop} = \frac{-j\left(Z_2 \tan\theta_2 + Z_3 \tan\theta_3\right)}{\left(\frac{Z_2}{Z_3} + \frac{Z_3}{Z_2}\right)\left(1 - \tan^2\left(\frac{\theta_2}{2}\right)\right)\left(1 - \tan^2\left(\frac{\theta_3}{2}\right)\right) + 4\left(\tan^2\left(\frac{\theta_2}{2}\right) + \tan^2\left(\frac{\theta_3}{2}\right)\right)}. \tag{7}$$

The condition required for the resonant to occur is when $Z_{od} = \infty$, thus, the resonant frequency of the resonator can be deduced as [17]:

$$\left(1 + R_Z^2\right)\left(1 - \tan^2\left(\frac{\theta_2}{2}\right)\right)\left(1 - \tan^2\left(\frac{\theta_3}{2}\right)\right) + 4R_Z\left(\tan^2\left(\frac{\theta_2}{2}\right) + \tan^2\left(\frac{\theta_3}{2}\right)\right) + \left(\tan\theta_2 + R_Z \tan\theta_3\right)\tan\left(\frac{\theta_1}{4}\right) = 0. \tag{8}$$

The electrical length ratio of the resonator is given as:

$$\alpha = (\theta_2)/(\theta_2 + \theta_3), \tag{9}$$

by substituting Eq. (9) into Eq. (8), any desired frequency ratio (f_s/f_0) of harmonic (f_s) to fundamental (f_0) resonances depends on the choice of suitable combination of the impedance and electrical length ratios of the resonator. The initial physical parameters of BPF1 and BPF2 can be obtained from Eqs. (9) to (11):

$$f_s/f_0 = 4\theta_s/\pi, \tag{10}$$

$$\theta_s = (\theta_2 + \theta_3)/2 = \theta_1/4. \tag{11}$$

From Eqs. (8) to (11), there are several solutions for θ_2 and θ_3, which depend on the choice of R_z and f_s/f_o. Fig. 1(d) depicts the normalized resonant frequency (f_s/f_o) against electrical length ratio (α). In this work, the resonator of BPF1 is chosen to operate at 8.3 GHz with $f_s/f_o = 0.9$, $R_z = 1.6$ ($Z_1 = Z_3 = 132.19\,\Omega$ and $Z_2 = 83.86\,\Omega$), and $\alpha = 0.23$ ($\theta_1 = 78°$, $\theta_2 = 9°$, and $\theta_3 = 30°$), while the resonator of BPF2 is designed at 10 GHz with $f_s/f_o = 1.5$, $R_z = 1.6$ ($Z_1 = Z_3 = 132.26\,\Omega$ and $Z_2 = 83.93\,\Omega$), and $\alpha = 0.13$ ($\theta_1 = 138°$, $\theta_2 = 9°$, and $\theta_3 = 60°$). It should be noted that the above calculation method does not mean that the parameters obtained will be exactly the desired frequency; therefore, a careful optimization should be performed.

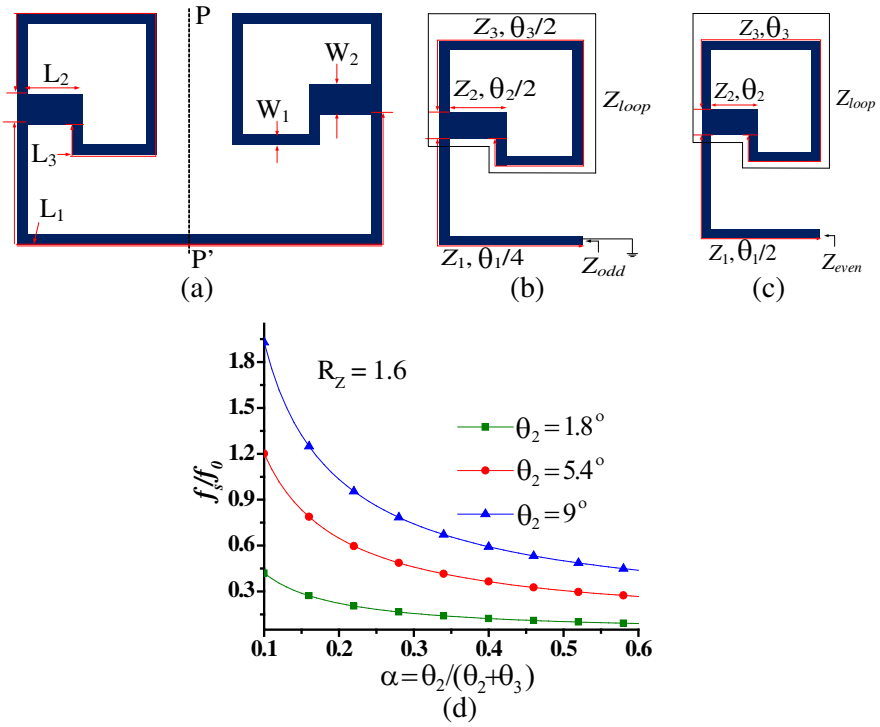

Figure 1. (a) Structure of the resonator, (b) odd-mode equivalent transmission-line model, (c) even-mode equivalent transmission-line model, and (d) the normalized resonant frequency (f_s/f_o) against the electrical length ratio (α).

2.2. Filter Design

Based on the above resonator analysis, two configurations of BPFs operating at 8.3/10 GHz, respectively, have been designed. The designed BPFs have been optimized using HFSS software. The BPF1 operating at 8.3 GHz should have a wide upper stopband in order to avoid the interference with the frequency response of BPF2. For the same reason, the BPF2 operating at 10 GHz should have a wide lower stopband in order to avoid the interference with the frequency response of BPF1 [18, 19]. To validate the proposed design concept, the design parameters of BPFs such as the 3-dB bandwidths (BWs) with 11% (BPF1) and 13 % (BPF2), the coupling coefficients and external quality factor can be determined regarding circuit elements of a second-order Chebyschev prototype filter. Based on approximate synthesis formulas [20] of the standard Chebyshev low-pass prototype filter, the elements are defined as: $g_0 = 1$, $g_1 = 0.9513$, $g_2 = 1.3630$, $J_1 = -0.1357$, and $J_2 = 1.0310$. According to the relationship between the bandpass design parameters and standard Chebyshev low-pass prototype filter

elements [20], the coupling matrices of the two passbands are deduced as:

$$M_{ij}^{BPF1} = \begin{bmatrix} 0 & 0.0966 & 0 & -0.01569 \\ 0.0966 & 0 & 0.0832 & 0 \\ 0 & 0.0832 & 0 & 0.0966 \\ -0.01569 & 0 & 0.0966 & 0 \end{bmatrix}, \tag{12}$$

$$M_{ij}^{BPF2} = \begin{bmatrix} 0 & 0.1142 & 0 & -0.01854 \\ 0.1142 & 0 & 0.0983 & 0 \\ 0 & 0.0983 & 0 & 0.1142 \\ -0.01854 & 0 & 0.1142 & 0 \end{bmatrix}, \tag{13}$$

where M_{ij}^{BPF1} and M_{ij}^{BPF2} are the coupling matrices of BPF1 and BPF2, respectively.

For each BPF, the coupling coefficient K is a function of parameter S. As seen in Fig. 2(c), the coupling coefficients of two passbands are decreased when the space S between the two resonators is increased. By using full-wave EM simulation software, the coupling coefficient K can be evaluated from the two dominant resonant frequencies for two coupled resonators. Assuming that f_{p1} and f_{p2} are the two splitting resonant mode frequencies, the coupling coefficient can be extracted using the following expression [20]:

$$K_{ij} = \left(f_{p2}^2 - f_{p1}^2\right) / \left(f_{p1}^2 + f_{p2}^2\right). \tag{14}$$

The external quality factor can be obtained by the following equation [20]:

$$Q_e = f_0 / \Delta f_{-3dB}, \tag{15}$$

where f_0 is the resonant frequency, and $\Delta f_{-3\,\mathrm{dB}}$ is a 3-dB BW of the input or output resonator when it is alone externally excited. Based on the above mentioned, the required coupling space (S) between two

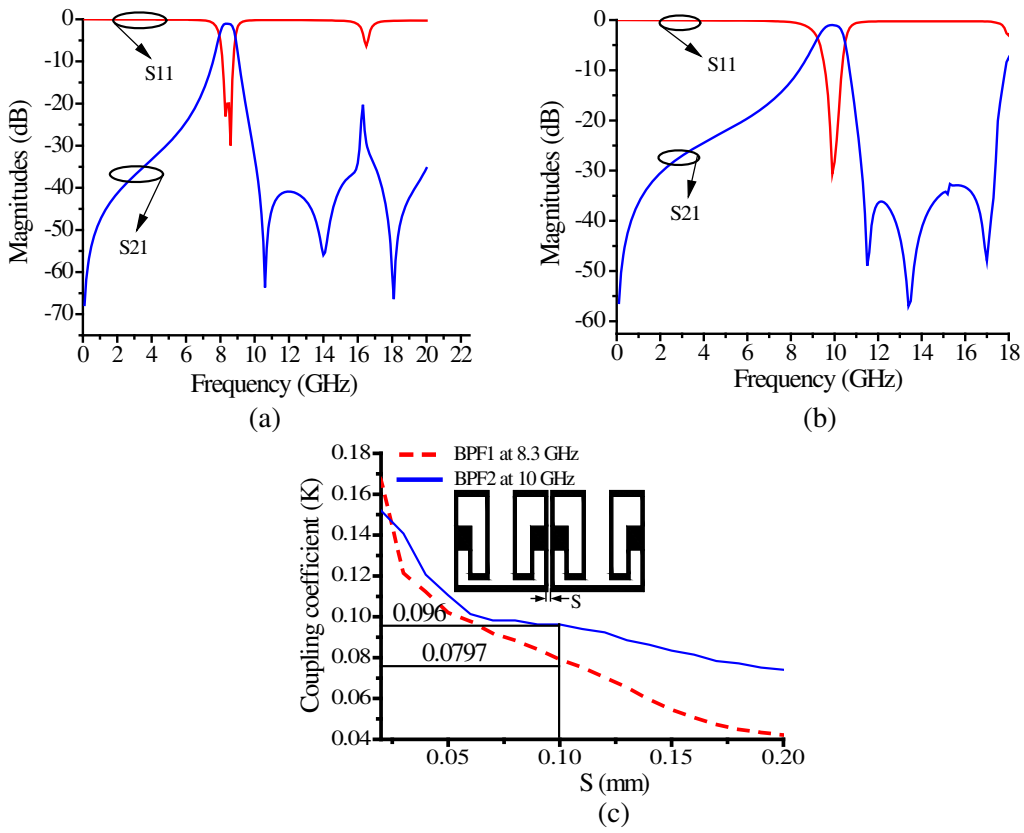

Figure 2. Simulated frequency response of the two BPFs and their coupling coefficient: (a) for BPF1 (at 8.3 GHz), (b) for BPF2 (at 10 GHz), and (c) Coupling coefficient for both of two BPFs.

resonators of each BPF to make proper coupling is 0.1 mm whereas the satisfactory coupling coefficient can be obtained as 0.0797 and 0.096 for BPF1 and BPF2, respectively. The desired external quality factors of BPF1 and BPF2 are 75.45 and 76.92, respectively. Figs. 2(a) and (b) indicate the simulated results of BPF1 and BPF2, respectively. The 3-dB fractional bandwidths (FBWs) for BPF1 and BPF2 are 11% and 13%, respectively. The simulated insertion loss within the passband of BPF1 is estimated as 1.03 dB, whereas its return loss is better than 20 dB. In the same way, the simulated insertion loss within the passband of BPF2 is about 1 dB, whereas its return loss is better than 30 dB.

2.3. Diplexer Design

The layout of the proposed microstrip diplexer is shown in Fig. 3. To construct a dual-channel diplexer, two BPFs shown in Fig. 3, whose passbands are corresponding to each channel of the diplexer, should be designed first. The second step is to combine the two BPFs based on DCLSIR. Each path of the diplexer is a two-order BPF. To combine two BPFs to form a diplexer, the most popular techniques used are the T-junction [2, 3], Y-junction [4, 5], common resonator [6, 7], and matching circuit [8, 9]. In this paper, T-junction technique is used to provide the input signal and impedance matching which has two branches. Each branch of the T-junction is linked to one of the two BPFs. The length $(L_6 + L_7)$ of the branch linked to lower BPF (BPF1) is approximated to a quarter of the guided wavelength of upper BPF (BPF2). In the same way, the length $(L_4 + L_5)$ of the branch connected to BPF2 is approximated to a quarter of the guide wavelength of BPF1. Finally, the proposed microstrip diplexer is obtained after carefully tuning the two branches.

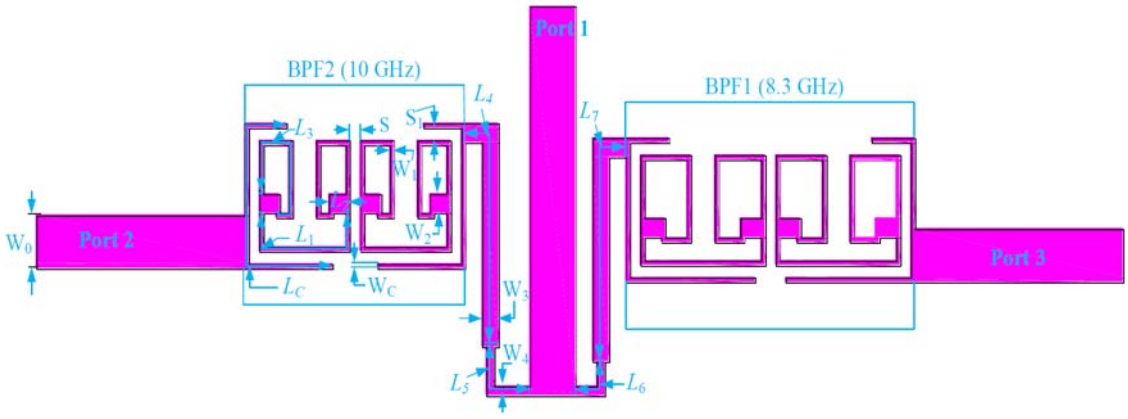

Figure 3. Layout of the proposed microstrip diplexer.

The optimized dimensions (all in mm) of the proposed diplexer, as depicted in Fig. 3, are: Common: $S = 0.1$, $S_1 = 0.1$, $W_0 = 1.1$, $W_1 = 0.1$, $W_2 = 0.4$, $W_3 = 0.4$, $W_4 = 0.2$, $W_c = 0.1$, BPF1: $L_1 = 3.93$, $L_2 = 0.6$, $L_3 = 4.83$, $L_6 = 1.2$, $L_7 = 5$, $L_c = 6.71$, BPF2: $L_1 = 3.55$, $L_2 = 0.5$, $L_3 = 3.205$, $L_4 = 5$, $L_5 = 1.85$, $L_c = 5.606$.

3. MEASURED RESULTS AND DISCUSSION

A prototype of the proposed microstrip diplexer has been designed and fabricated on a dielectric substrate with $\varepsilon_r = 3.66$, $h = 0.508$ mm, and $\tan\delta = 0.004$. The design of the structure and simulation of the proposed microstrip diplexer have been carried out by using HFSS software. A photograph of the fabricated microstrip diplexer is shown in Fig. 4 with the merit of a compact size of 15.17 mm $\times$ 2.69 mm. In terms of wavelength, the size without the 50 Ω feed lines can be approximated as $0.657\lambda_g \times 0.117\lambda_g$, where λ_g is the guided wavelength at the first passband. The measurement results of the proposed microstrip diplexer are obtained by using Agilent N5244A Vector Network Analyzer. As shown in Fig. 5, the agreement between simulated and measured results is good. However, the observed deviation between the simulated and measured results might be due to fabrication errors. The simulated in-band

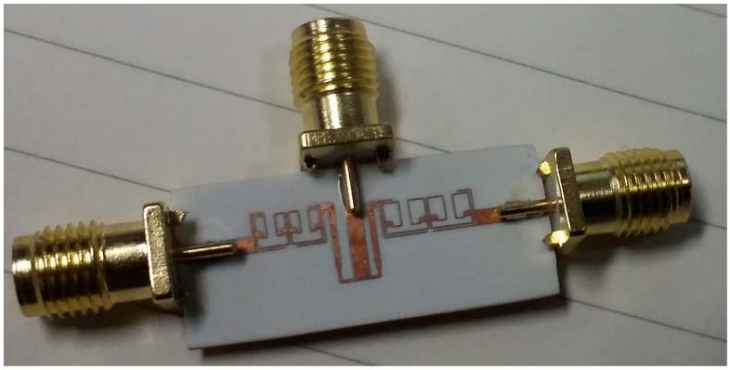

Figure 4. The photograph of the fabricated microstrip diplexer.

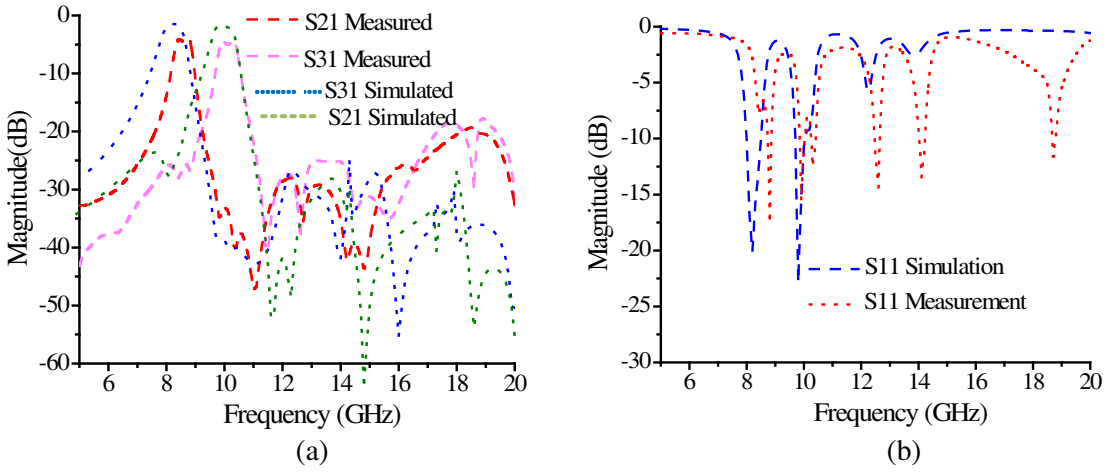

Figure 5. Simulated and measured frequency responses of the dual-channel diplexer: (a) Simulated and measured frequency responses for S_{21} and S_{31} and (b) simulated and measured frequency responses for S_{11}.

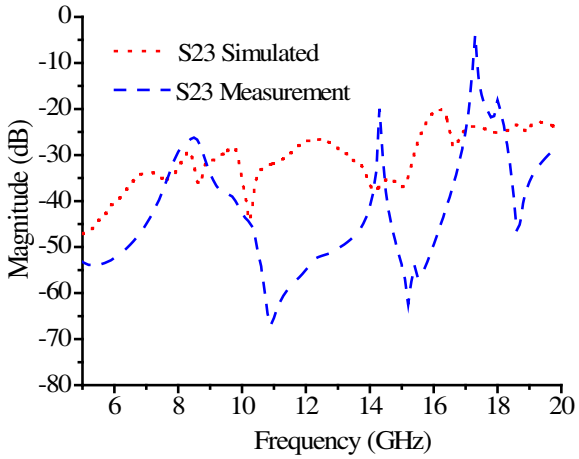

Figure 6. Simulated and measured isolation responses.

insertion losses at lower and higher passbands are 1.3 dB and 1.45 dB, respectively, whereas its measured in-band insertion losses at lower and higher passbands, including the loss from SMA connectors, are about 1.8 and 1.9 dB. The simulated in-band return losses at the first and second passbands are 20 dB and 23 dB, respectively, whereas its measured in-band return losses at the first and second passbands, including the loss from SMA connectors, are better than 10 dB. The 3-dB FBWs of the channels are 11% (BPF1) and 13% (BPF2). It should be noted that some displacements of the central frequencies of the lower and upper passbands led to this. This shifting produces a slight reduction of the channels' bandwidths but does not affect their selectivity. The observed disagreements at central frequencies far from the passbands might be because second order effects are not taken into account by the parametric models. Moreover, for good impedance matching, the isolation between the two channels as depicted in Fig. 6 is 26.69 dB. The small discrepancy observed between the simulated and measured results might be due to fabrication errors. Table 1 depicts the performance comparison between the proposed microstrip diplexer and reported diplexers. Compared with other approaches as indicated in Table 1, the proposed microstrip diplexer has advantages of low insertion loss, good isolation, and compact size.

Table 1. Comparison between the proposed and previous diplexers.

Ref.	CFs (GHz)	$1^{st}/2^{nd}$ IL (dB)	$1^{st}/2^{nd}$ RL (dB)	Iso. (dB)	$1^{st}/2^{nd}$ FBW (%)	Circuit size $(\lambda_g \times \lambda_g)/(mm^2)$
[9] Fig.7	2.36/5.17	2.3/2.8	-	18	7.6/6.4	0.89 x 0.50/ 61.85 x 34.7
[10]	1.75/1.95	1.95/1.8	10/12	20	5.71/5.13	0.35 x 0.40/ 43.50 x 56.60
[11]	1.80/2.45	2.05/2.15	15/15	25	-	0.20 x 0.18/ 50 x 53
[12]	2.4/2.6	2.24/3.17	12.4/17.86	15	-	1.59 x 0.81/ 134 x 68.47
[13]	2.4/5.2	1.94/2.55	10.8/12	25	12.5/5.9	0.50 x 0.95/ 35 x 23.16
[14]	1.8/2.45	2.2/1.8	17/16	21	8.75/6	0.25 x 0.65/ 20 x 52
[15]	1.75/1.85	2.1/2.1	20/20	20	-	0.47 x 0.15/ 54 x 17
This work	**8.3/10**	**1.8/1.9**	**10/10**	**26.69**	**11/13**	**0.65 x 0.11/ 15.17 x 2.69**

Ref., References; CFs, Central frequencies; IL, Insertion loss; RL, Return loss; Iso., Isolation; FBW, Fractional bandwidth

4. CONCLUSION

In this paper, a compact microstrip diplexer based on DCLSIR has been presented. The proposed microstrip diplexer is composed of two channels based on DCLSIR operating at (8.3)/(10) GHz. The circuit size of the fabricated microstrip diplexer is estimated $0.657\lambda_g \times 0.117\lambda_g$, where λ_g is the guided wavelength at the first passband. Due to an appropriate choice of DCLSIR geometry, a compact size, low insertion loss, good isolation between the two channels, and low cost have been achieved. Based on the above mentioned advantages, the proposed microstrip diplexer has a good potential application in X-band systems.

ACKNOWLEDGMENT

The work for this grant was supported by the National Natural Science Foundation of China (Grant No. U1430102). The authors also would like to thank Dr. Boukarkar Abdelheq from the University of Electronic Science and Technology of China, school of electronic science and engineering, for his great assistance in the revision of this paper.

REFERENCES

1. Yao, H. W., A. E. Abdelmonem, J. F. Liang, X. P. Liang, K. A. Zaki, and A. Martin, "Wide-band and ridge waveguide T-junctions for diplexer applications," *IEEE Trans. Microw. Theory. Tech.*, Vol. 41, 2166–2173, 1993.
2. Sirci, S., J. D. Martinez, J. Vague, and V. E. Boria, "Substrate integrated waveguide diplexer based on circular triplet combine filters," *IEEE Microw. Wirel. Compon. Lett.*, Vol. 25, 430–432, 2015.
3. Li, K.-H., C.-W. Wang, and C.-F. Yang, "A miniaturized diplexer using planar artificial transmission lines for GSM/DCS applications," *Asia-Pacific Microwave Conference*, 1–4, 2007.
4. Zhao, C., C. Fumeaux, and C. C. Lim, "Substrate-integrated waveguide diplexers with improved Y-junctions," *Microwave. Op. Technol. Lett.*, Vol. 58, 1384–1388, 2016.
5. King, T. S., A. T. Y. Ying, and S. H. Tiong, "A microstrip diplexer using folded hairpins," *IEEE International RF and Microwave Conference*, 226–229, 2011.
6. Tantiviwat, S., N. Intarawiset, and R. Jeenawong, "Wide-stopband, compact microstrip diplexer with common resonator using stepped-impedance resonators," *IEEE Tencon-Spring Conference*, 174–177, 2013.
7. Chen, C.-F., T.-Y. Huang, C.-P. Chou, and R.-B. Wu, "Microstrip diplexers design with common resonator sections for compact size, but high isolation," *IEEE Trans. Microw. Theory Tech.*, Vol. 54, 1945–1952, 2006.
8. Zhu, C., L. Yao, and J. Zhou, "Novel microstrip diplexer based on a dual-band bandpass filter for WLNA system," *Asia-pacific Microwave Conference*, 1102–1105, 2010.
9. Deng, P.-H., C.-H. Wang, and C. H. Chen, "Compact microstrip diplexer based on a dual-passband filter," *Asia-Pacific Microwave Conference*, 1–5, 2006.
10. Choocadee, S., N. Intarawiset, and S. Tantiviwat, "Compact microstrip diplexer using triple-mode stub loaded resonators," *IEEE MTT-S International Conference on Microwave for Intelligent Mobility*, 9–12, 2017.
11. Liu, H., W. Xu, Z. Zhang, and X. Guan, "Compact diplexer using slotline resonator," *IEEE Microw. Wirel. Compon. Lett.*, Vol. 23, 75–77, 2013.
12. Baba, N. H., A. H. Awang, M. T. Ali, M. A. Aris, and H. M. Hizan, "Design of a SIW-based microstrip diplexer using TM_{010} circular cavity," *Theory and Applications of Applied Electromagnetics*, 71–79, 2016.
13. Chen, C. M., S. J. Chang, and C. F. Yang, "Fabrication of a novel diplexer using folded open-loop ring resonators and microstrip lines," *ACES Journal*, Vol. 29, 864–869, 2014.

14. Chinig, A., J. Zbitou, A. Errkik, A. Tajmouati, L. EI Abdellaoui, M. Latract, and A. Triback, "Microstrip diplexer using stepped impedance resonators," *Wireless Personal Communication*, Vol. 84, 2537–2548, 2015.
15. Peng, H. S. and Y. C. Chiang, "Microstrip diplexer constructed with new types of dual-mode ring filters," *IEEE Microwave Wirel. Compon. Lett.*, Vol. 25, 7–9, 2015.
16. Xue, Q. and J.-X. Chen, "Compact diplexer based on double-sided parallel-strip line," *Electron. Lett.*, Vol. 44, 123–124, 2008.
17. Dembele, S. N., T. Zhang, J. Bao, and D. Bukuru, "Compact microstrip bandpass filter using dual closed-loop stepped impedance resonator," *Int. J. Microw. Wirel. Technol.*, Vol. 10, 405–411, 2018.
18. Huang, C.-Y., M.-H. Weng, C.-S. Ye, and Y.-X. Xu, "A high band isolation and wide stopband diplexer using dual-mode stepped-impedance resonators," *Progress In Electromagnetics Research*, Vol. 100, 299–308, 2010.
19. Ye, C.-S., Y.-K. Su, M.-H. Weng, and C.-Y. Hung, "A microstrip ring-like diplexer for Bluetooth and UWB application," *Microw. Op. Technol. Lett.*, Vol. 51, 1518–1520, 2009.
20. Hong, J.-S. and M. J. Lancaster, "Design of highly selective microstrip bandpass filters with a single pair of attenuation poles finite frequencies," *IEEE Trans. Microw. Theory Tech.*, Vol. 48, 1098–1107, 2000.